PCCP

PAPER

Adsorption and separation of binary and ternary mixtures of SO_2, CO_2 and N_2 by ordered carbon nanotube arrays: grand-canonical Monte Carlo simulations

Mahshid Rahimi,*[a] Jayant K. Singh[ab] and Florian Müller-Plathe[a]

The adsorption and separation behavior of SO_2–CO_2, SO_2–N_2 and CO_2–N_2 binary mixtures in bundles of aligned double-walled carbon nanotubes is investigated using the grand-canonical Monte Carlo (GCMC) method and ideal adsorbed solution theory. Simulations were performed at 303 K with nano-tubes of 3 nm inner diameter and various intertube distances. The results showed that the packing with an intertube distance $d = 0$ has the highest selectivity for SO_2–N_2 and CO_2–N_2 binary mixtures. For the SO_2–CO_2 case, the optimum intertube distance for having the maximum selectivity depends on the applied pressure, so that at $p < 0.8$ bar $d = 0$ shows the highest selectivity and at 0.8 bar $< p < 2.5$ bar, the highest selectivity belongs to $d = 0.5$ nm. Ideal adsorbed solution theory cannot predict the adsorption of the binary systems containing SO_2, especially when $d = 0$. As the intertube distance is increased, the ideal adsorbed solution theory based predictions become closer to those of GCMC simulations. Only in the case of CO_2–N_2, ideal adsorbed solution theory is everywhere in good agreement with simulations. In a ternary mixture of all three gases, the behavior of SO_2 and CO_2 remains similar to that in a SO_2–CO_2 binary mixture because of the weak interaction between N_2 molecules and CNTs.

1. Introduction

In the last decade carbon nanotubes (CNTs) have been widely studied as adsorbents of different gases such as H_2, N_2, CO_2, SO_2, alkanes and noble gases.[1,2] This great interest in using CNTs for gas adsorption and separation is mainly due to their hollow cylindrical geometry, low mass density and large specific area.[3,4] In many studies, CNTs were compared with other gas sorbents and found to have higher gas adsorption and separation. Lu et al. studied CO_2 capture experimentally and showed that CNTs are better adsorbents in terms of capacity per mass, compared with other sorbents such as zeolites and activated carbon.[5] Diffusivities of light gases (H_2 and CH_4) in carbon nanotubes and zeolites with comparable pore sizes were studied by molecular dynamics simulations. It was found that the diffusivity of H_2 and CH_4 in carbon nanotubes is orders of magnitude faster than in zeolites.[6] Using grand canonical Monte Carlo (GCMC) simulations for CO_2 and CH_4 adsorption, Huang et al. showed that CNTs have a higher selectivity for CO_2/CH_4

separation than that reported for activated carbons, zeolite 13X and metal organic frameworks (MOFs).[7]

The important role of carbon porosity was revealed by simulated SO_2 adsorption isotherms on activated carbon.[8] This role is even more important in the case of CNTs because of their well-defined structure and arrangement. Accordingly, the optimization of the geometrical properties like the tube dia-meter and the intertube distance has always been a question. Jakobtorweihen et al.[9] employed GCMC simulations to investi-gate the adsorption of linear alkanes and alkenes on CNTs with different tube diameters. Narrower pores were found to have higher adsorption at low pressure ($p < 2$ bar) and lower adsorp-tion at high pressure (2 bar $< p < 1000$ bar). Kowalczyk and coworkers[10] used GCMC to measure the amount of CO_2 adsorbed onto CNTs and showed that the optimum diameter for having the highest adsorption depends on the applied pressure. This result was confirmed by our recent study of SO_2 adsorption on CNTs.[11] The same method has been used to measure the adsorption of CO_2 and SO_2 molecules on single-walled CNTs (SWCNTs).[12] The contributions of the inner and outer adsorption were studied and it was found out that for both molecules, the inside adsorption is higher at low pressures. The outside adsorption becomes larger above 10 and 2 bar for CO_2 and SO_2, respectively.

In CNT bundles, the intertube distance is a second geo-metrical parameter that can be tuned[13] and it is also claimed to

[a] Technische Universität Darmstadt, Eduard-Zintl-Institut für Anorganische und Physikalische Chemie, Alarich-Weiss-Str. 4, D-64287 Darmstadt, Germany. E-mail: mahshid.rahimi@theo.chemie.tu-darmstadt.de

[b] Department of Chemical Engineering, Indian Institute of Technology Kanpur, Kanpur-208016, India

4112 | Phys. Chem. Chem. Phys., 2016, 18, 4112–4120

This journal is © the Owner Societies 2016

have an important effect on adsorption.[14,15] Agnihotri et al.[16] combined the experiment and simulations to analyze the adsorption sites in CNT bundles. They showed that grooves are the most favorable sites. They are completely filled already at very low pressure. In order to measure the adsorption locally, Bienfait and coworkers[17] used neutron diffraction measurements of different gases on CNTs. They also found grooves as the best adsorption sites.

The ideal adsorbed solution theory (IAST) developed by Myers and Prausnitz[18] is a technique used to calculate multi-component adsorption equilibria based on single-component adsorption isotherms. The agreement of IAST and GCMC simulations for the adsorption of binary mixtures of $CO_2/CH_4/H_2/N_2$ on various materials, like MOFs and CNTs, was confirmed by various groups.[19–21] Cannon and coworkers[22] used GCMC to study the adsorption and selectivity of linear alkanes on closed nanotube bundles. They found that the adsorption of the alkane mixture agrees between IAST and simulations. Peng et al.[23] showed that the IAST prediction of CO_2 and CH_4 adsorption in ordered carbon nanopipes is in good agreement with experiment. Using molecular simulations and IAST, the selectivity of nanoporous carbon materials for the mixture of CO_2 and H_2 was studied by Kumar and Rodríguez-Reinoso.[24] To investigate the effects of nanopore structure, carbon nanotubes, slit-shaped porous carbon form and a carbon model with a disordered pore structure, were considered. The results showed that CNTs have the highest selectivity towards CO_2.

Among all the adsorption and separation studies, there are few investigations of SO_2 and its mixture with CO_2. Wang and coworkers[25] used GCMC to calculate SO_2–CO_2 and SO_2–N_2 mixtures in CNT bundles with different tube diameters. They found that among the studied diameters, 1.09 nm and 0.81 nm show the highest selectivity for SO_2–CO_2 and SO_2–N_2 respectively. Furthermore, they showed a decrease of selectivity with increasing temperature. The observations of these authors were still based on bundles of single-walled CNTs (SWCNTs) with a fixed intertube distance. However, it is not known if such behavior also occurs for double- or multi-walled CNT bundles. Moreover, the effect of the intertube distance was not investigated. Finally, it would be helpful for experimental studies to know if IAST can be used for the adsorption of the SO_2–CO_2 mixture in bundles of CNTs.

In this study, we investigate the adsorption and selectivity of binary (SO_2–CO_2, CO_2–N_2 and SO_2–N_2) and ternary mixtures (SO_2–CO_2–N_2) in bundles of double-walled carbon nanotubes (DWCNTs) using the GCMC method. Since the influence of the tube diameter has been exhaustively studied,[11,26] the intertube distances of DWCNT arrays are varied in order to find the optimum geometry for each adsorption/separation situation. Predictions of the IAST approximation are compared with the results of the simulations.

2. Model and method

Following our previous studies,[14,15,26] the DWCNTs in the simulation box are arranged on a hexagonal lattice, and periodic boundary conditions are used in all three directions (cf. Fig. 1 of ref. 14). In the present study, DWCNTs with an inner tube diameter of $2R = 2.98$ nm, which was found to be optimum for single gas adsorption, are used.[26] Since the adsorption isotherm was found to be insensitive to the CNT length,[11] the DWCNT length is fixed to be 7.38 nm. The intertube distance (the surface to surface distance between the outer layers of adjacent tubes, i.e. $d = 0$ represents the case of touching DWCNTs, the distance between the positions of their surface carbons being 0.34 nm) is varied ($d = 0$ to 2 nm), since it has a stronger effect compared to the tube diameter, and since its optimum value depends on the applied pressure.[11] The simulation box length in the direction of the CNT axes is equal to the CNT length; the simulation box lengths in the other two directions are adjusted to the intertube distance. In total, there are 11 760 carbon atoms in the simulation box.

The DWCNTs are considered as rigid structures with a C–C bond length of 0.142 nm. The Lennard-Jones potential of the AMBER96 force field[27] is used to describe DWCNTs. It has been used in similar work.[11,28] The EPM2 model of Harris and Yung[29] is used to describe CO_2. In this model, CO_2 is considered as a 3-site rigid molecule with Lennard-Jones potential ($\sigma_{C-C} = 0.2757$ nm, $\varepsilon_{C-C} = 0.23388$ kJ mol^{-1}, $\sigma_{O-O} = 0.3033$ nm, $\varepsilon_{O-O} = 0.66837$ kJ mol^{-1}) plus a set of partial point charges ($q_C = 0.6512e$), a fixed bond length ($l_{C-O} = 0.1149$ nm) and a fixed angle ($\theta_{O-C-O} = 180°$). Ketko et al.[30] developed an optimized intermolecular potential for SO_2 to accurately calculate the vapor–liquid equilibria, critical properties, vapor pressure, and heats of vaporization. This rigid model, which is used in the present study, describes SO_2 using Lennard-Jones interactions and partial charges ($\sigma_{S-S} = 0.339$ nm, $\varepsilon_{C-C} = 0.61361$ kJ mol^{-1}, $\sigma_{O-O} = 0.305$ nm, $\varepsilon_{O-O} = 0.65684$ kJ mol^{-1}, $l_{S-O} = 0.1432$ nm, and $\theta_{O-S-O} = 119.3°$). The N_2 molecules are also modeled as a 3-site molecule with Lennard-Jones potential plus a set of partial point charges, a fixed bond length and a fixed angle.[31] Dissimilar non-bonded interactions are calculated using the Lorentz–Berthelot combining rules. The electrostatic interactions are calculated using the smooth-particle-mesh Ewald (SPME) method.[32]

The grand canonical Monte Carlo method at constant chemical potential μ, volume V and temperature T is used to calculate the adsorption and separation coefficients of gases. Three Monte Carlo moves, displace, rotate, and insert/delete, with the probability of 0.2, 0.1 and 0.7, respectively, are implemented. The temperature is fixed at 303 K and the atomic cutoff is 1 nm. In order to account for the non-ideality of gases, the fugacities of the components in the bulk phases were calculated using the Peng–Robinson equation of state (PR EOS) for mixtures.[33] For all simulation runs, 1×10^7 Monte Carlo steps are used for equilibration and another 1×10^7 Monte Carlo steps for data collection. The output of the simulation is the total number of gas molecules of each component, which is converted to a common unit for adsorption, mmol of gas per gram of adsorbent and is denoted n_i for the component i. Adsorption selectivity of component i relative to component j in a binary system is calculated using

$$S_{i/j} = \left(\frac{x_i}{y_i}\right) \Big/ \left(\frac{x_j}{y_j}\right) \tag{1}$$

This journal is © the Owner Societies 2016

Phys. Chem. Chem. Phys., 2016, **18**, 4112–4120 | **4113**

where x_i and y_i are the molar fractions of component i in the adsorbed and bulk gas phases, respectively.

The composition of flue gas strongly depends on the type of fuel and the combustion conditions. For instance, the flue gas from coal-fire consists of 7 to 15% moles of CO_2.[34,35] In this work, we use the molar ratio of 5:95, 1:99 and 15:85 in the bulk phase for the binary mixtures of SO_2–CO_2, SO_2–N_2, and CO_2–N_2, respectively.[25,36–38]

The ideal adsorbed solution theory (IAST) predicts multi-component sorption equilibria from single-component isotherms.[18] According to IAST, the following equation holds for each component of the studied mixture based on an analogy with Raoult's law:

$$py_i = x_i p_i(\pi), \qquad (2)$$

where p is the total pressure in the bulk gas phase, p_i is the bulk pressure of component i that corresponds to the spreading pressure π of the binary mixture; and x_i and y_i have been explained above (eqn (1)). Since the molar fractions of the adsorbed species sum to one, eqn (2) can be written as

$$\frac{py_1}{p_1} + \frac{py_2}{p_2} = 1, \qquad (3)$$

for each component; p_i and π are related through

$$\frac{\pi A}{RT} = \int_0^{p_i} \frac{n_i(p)}{p} dp, \qquad (4)$$

where A is the surface area of the adsorbent, R is the universal gas constant, T denotes temperature, and $n_i(p)$ is the amount adsorbed at pressure p.

Levan and Vermeulen used eqn (2)–(4) together with the single-component Langmuir isotherms to derive an explicit and thermodynamically consistent binary Langmuir isotherm.[39,40] The adsorption isotherm of each pure component is simulated individually using GCMC. Then it is fitted using the Langmuir isotherm

$$n_i^0 = \frac{n_{i,\max}^0 K_i p}{1 + K_i p}, \qquad (5)$$

where $n_{i,\max}^0$ is the monolayer capacity, K_i is the constant in the Langmuir isotherm and n_i^0 is the adsorbed amount of component i in a single-component system. The fitted parameters and eqn (2)–(4) are used to calculate the adsorption of component i, n_i, in a binary mixture

$$n_1 = \frac{QP_1^*}{1 + P_1^* + P_2^*} + \left(n_{1,\max}^0 - n_{2,\max}^0\right)\frac{P_1^* P_2^*}{(P_1^* + P_2^*)^2}\ln(1 + P_1^* + P_2^*), \qquad (6)$$

$$n_2 = \frac{QP_2^*}{1 + P_1^* + P_2^*} + \left(n_{2,\max}^0 - n_{1,\max}^0\right)\frac{P_1^* P_2^*}{(P_1^* + P_2^*)^2}\ln(1 + P_1^* + P_2^*). \qquad (7)$$

The dimensionless parameter P_i^* is defined as $P_i^* = K_i p_i$, and Q is the weighted monolayer capacity and can be calculated using

$$Q = \frac{n_{1,\max}^0 P_1^* + n_{2,\max}^0 P_2^*}{P_1^* + P_2^*}. \qquad (8)$$

3. Results and discussion

3.1. SO₂–CO₂ mixture

Fig. 1 shows the adsorption isotherms of a mixture of SO_2 and CO_2 at a molar ratio of 5:95 on a bundle of 3 nm diameter DWCNTs as a function of the total bulk pressure. For CO_2 (Fig. 1a), the system with $d = 0.5$ nm shows the highest adsorption in the studied pressure range. The reason is the direct relationship between d and adsorption energy, and the inverse relationship between d and accessible volume. The competing effects of adsorption energy and adsorption space volume cause $d = 0.5$ nm to be the optimum intertube distance for having the maximum adsorption in this pressure range (0.1 bar $< p <$ 2.5 bar). The bulk partial pressure of CO_2 (p_{CO_2}) varies with the total pressure of the particle reservoir. It is in the range 0.095 to 2.375 bar. The optimum intertube distance, within this partial pressure range, for the maximum adsorption amount is similar to that of pure CO_2.[26] For SO_2 (Fig. 1b) at low pressure $p <$ 0.5 bar, $d = 0$ has the highest adsorption because there is a strong interaction between SO_2 molecules and CNT walls in the interstitial and groove regions when $d = 0$. Since the partial pressure of SO_2 is very low (0.005 bar $< p_{SO_2} <$ 0.025 bar), these regions have enough volume to accommodate the SO_2 molecules. As the pressure increases to $\sim$0.5 bar (partial pressure of SO_2 is $\sim$0.025 bar), the intertube volume is saturated and the optimal intertube distance is slightly shifted up to $d = 0.5$ nm. This trend continues up to the highest studied pressure in the present work ($p = 2.5$ bar) and CNT arrays with $d = 0.5$ nm have the highest adsorption between 0.5 bar and 2.5 bar. It is expected, however that a further increase of pressure will shift the
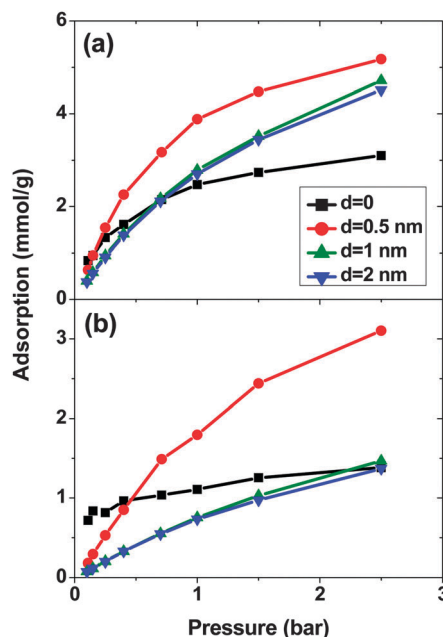

Fig. 1 Excess adsorption isotherms of (a) SO_2 and (b) CO_2 in a SO_2–CO_2 (5:95) binary mixture system on double-walled carbon nanotube arrays, with an inner tube diameter $2R = 3$ nm and an intertube distance $d = 0$–2 nm. $T = 303$ K. Pressure refers to the total pressure of the SO_2–CO_2 mixture.

optimal intertube distance to even higher values, as seen in earlier work for the adsorption of pure SO_2.[11] Moreover, it was found in the earlier studies[11,26] for a pure SO_2 system, that the maximum adsorption at low pressures is achieved for $d = 0.3$ nm[11] and $d = 0.5$[26] nm. Our results do not contradict these findings, since the lowest pressure studied in the previous studies was $p_{SO_2} \sim 0.1$ bar, but not the very low pressure region (0.005 bar $< p_{SO_2} < 0.125$ bar) of this work. Furthermore, our results confirm the previous finding that the optimum intertube distance depends on the applied pressure and the optimum d is shifted to higher values with increasing pressure.[11]

As expected, for all conditions CO_2 has higher adsorption than SO_2 due to its higher bulk concentration (95 mol%). However, the selectivity of SO_2 over CO_2 shows a non-uniform behavior (Fig. 2). When $d = 0$, the system shows the highest selectivity ($S_{SO_2/CO_2} = 16$) at very low pressure, since molecules perfectly fit to the narrow intertube pores of DWCNTs. Increasing the pressure to $p = 0.7$ bar leads to a decrease of the selectivity to around 8. With a further increase of the pressure, the selectivity remains almost constant ($S_{SO_2/CO_2} \sim 8$). The situation for the intertube distance of $d = 0.5$ nm is almost reversed. The selectivity increases strongly with pressure up to $p = 0.7$ bar, then it continues increasing but very smoothly. As a result, the two curves cross at $p \sim 0.8$ bar. The two systems with $d = 1$ and 2 nm show a behavior qualitatively similar to $d = 0.5$ nm. The selectivity increases smoothly over the whole studied pressure region, but does not exceed 6. Consequently, at lower pressure ($p < 0.8$ bar) $d = 0$ has the highest selectivity, while the highest selectivity at higher pressure (0.8 bar $< p < 2.5$ bar) is found for the system with $d = 0.5$ nm. The selectivity found by Wang et al.[25] for SWCNTs with similar inner diameters ($2R = 2.71$ nm) varies from ~ 10 to ~ 20 at different pressures and it is obviously higher than that found in the present study for DWCNTs. This is most likely due to the higher outer diameter of our DWCNTs ($2R_{out} = 3.66$ nm) and consequently, their larger intertube volume which leads to a decrease in adsorption energy. Moreover, it was also reported f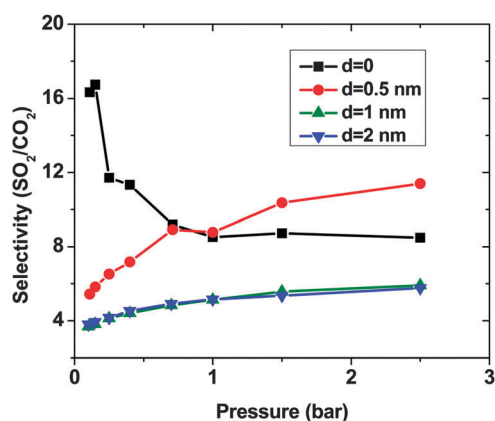or single-gas adsorption that SWCNTs show higher adsorption than DWCNTs.[41] DWCNTs, however, are still attractive from an application view point, since SWCNTs are expensive and more difficult to synthesise.[42] Moreover, the selectivity value is found here to range from 4 to 16, indicating that the optimization of the pore size tuning can increase it by 4 times.

At low pressure, CO_2 and SO_2 may adsorb separately without interfering with each other.[43] In order to verify this assertion, separate simulations are performed for pure SO_2 and CO_2 with the pressure same as the partial pressure in the binary mixture. Fig. 3 shows the SO_2 and CO_2 adsorption as a function of their partial pressure in three different situations: a single-component system, a binary system and IAST prediction. When $d = 0$, the IAST prediction does not agree with the simulation data, neither for CO_2 nor for SO_2. This means that, in the adsorbed phase, SO_2 and CO_2 molecules do not behave as an ideal mixture because of their high density in the low intertube space volume of this geometry. The GCMC results show higher SO_2 adsorption and lower CO_2 adsorption than the IAST prediction, reflecting the high selectivity for SO_2 of this system (Fig. 2). Furthermore, the adsorption of single gases deviates markedly from the adsorption of each component in the binary mixture. Thus, the assumption that each gas is adsorbed separately without interfering with the other is evidently not true in the CNT arrays with $d = 0$. There are also deviations between IAST predictions and the GCMC adsorption isotherms
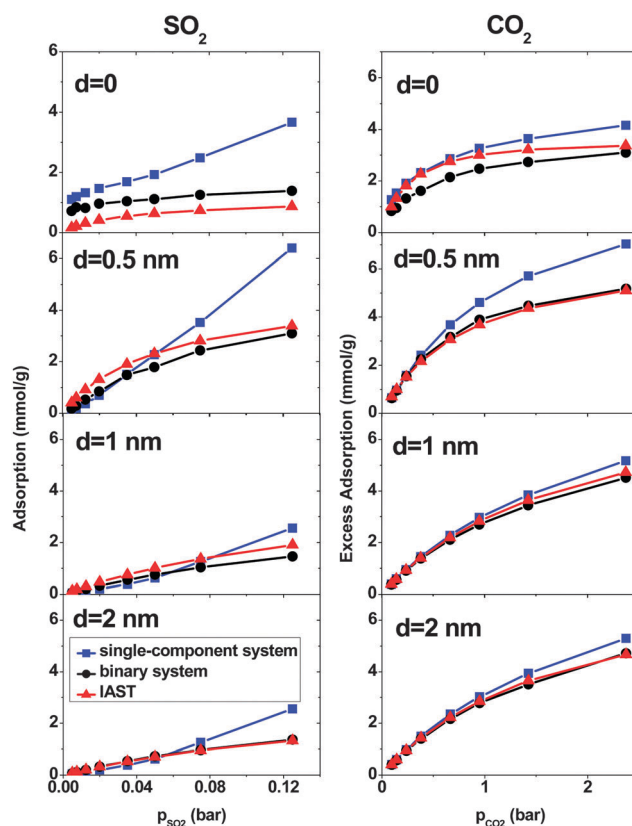

Fig. 2 Selectivity of SO_2 over CO_2, computed by the GCMC method, in a SO_2–CO_2 (5:95) binary mixture on double-walled carbon nanotube arrays, with the inner tube diameter $2R = 3$ nm and the intertube distance $d = 0$–2 nm. $T = 303$ K.

Fig. 3 Comparison of different methods in calculating the adsorption of SO_2 (left column) and CO_2 (right column) in a binary mixture system on double-walled carbon nanotube arrays, with the inner tube diameter $2R = 3$ nm and the intertube distance $d = 0$–2 nm. $T = 303$ K.

of single gases because the IAST predicts that each component occupies a certain amount of volume and as a result, the accessible volume in the IAST prediction for the other component is less than in single-gas systems. With increasing intertube distance, IAST predictions for the adsorption isotherms move closer to the simulation results, so that for $d = 2$ nm, the difference between adsorbed amounts predicted by IAST and simulation is less than 5% for CO_2 at $p_{CO_2} = 2.375$ bar and also for SO_2 at $p_{SO_2} = 0.125$ bar. This is due to the reduction of the gas density with increasing intertube distance. Adsorption isotherms of the binary system and single-component systems show the same trend with increasing d. For instance, at $p_{CO_2} = 0.66$ bar, the deviations between the adsorption of CO_2 in the binary system and the single-component system are 13%, 8% and 7% for $d = 0.5$ nm, 1 nm and 2 nm, respectively. Moreover, for $d > 0$, there is only a small deviation between the adsorption isotherms of the binary system and that of a single-component system at low pressure (*e.g.* for CO_2, $d = 2$ nm, at $p_{CO_2} = 0.38$ bar, the deviation is $\sim 5\%$). Increasing the pressure enhances the deviation so that for $d = 2$ nm, at $p_{CO_2} = 2.375$ bar, the difference between adsorption in the binary system and the single-component system is $\sim 13\%$. Therefore, at very low pressure, the two gases behave independently. However, at higher pressure, each gas occupies a considerable amount of volume and reduces the accessible volume for the other one and, hence, the presence of one gas has a detrimental effect on the adsorption of the other.

Fig. 4 shows the density profiles of CO_2 and SO_2 in systems with different d and p. The density profile inside the CNT is indifferent to d, as has been observed before for pure CO_2 and SO_2 adsorption.[11,14] In all systems, a layer of CO_2 and SO_2 forms at low pressure ($p = 0.4$ bar). This layer grows in density with increasing pressure. Outside the CNT, when $d = 0$, the density of SO_2 is higher than that of CO_2 at low pressure. As the pressure increases, the density of SO_2 remains almost constant but the density of CO_2 increases, confirming what has been observed for the selectivity in Fig. 2. The reduction in selectivity is due to the outer intertube volume being small and SO_2 being a large molecule. Therefore, the intertube volume saturates soon. The CO_2 molecules are smaller and they can fit themselves in the remaining space. For $d = 0.5$ nm, the densities of both CO_2 and SO_2 increase with pressure. The increase is larger for SO_2 than for CO_2, because the intertube space is larger, and SO_2 molecules interact strongly with CNT carbon molecules than CO_2. A similar behavior is observed for the case of $d = 1$ nm.

3.2. SO_2–N_2 mixture

Fig. 5 presents SO_2 and N_2 adsorption isotherms of a SO_2–N_2 (1 : 99) mixture. When $d = 0$, a remarkable increase of SO_2 adsorption can be seen until $p \sim 0.4$ bar. Beyond that, the adsorption approaches saturation with a lower rate. Increasing d leads to a drastic reduction in SO_2 adsorption and, hence, $d = 0$ has the highest adsorption in the studied pressure region. This is due to the strong interaction between SO_2 molecules
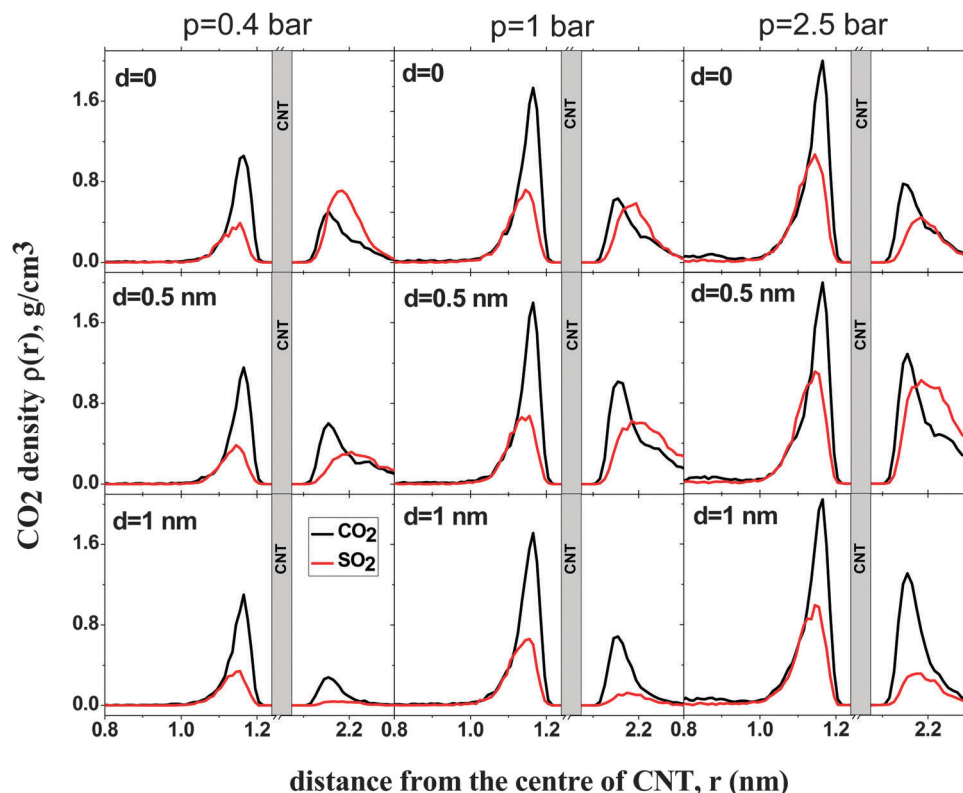

Fig. 4 Density profiles for SO_2 (red) and CO_2 (black) adsorption in a binary mixture (5 : 95) on double-walled carbon nanotubes, with the inner tube diameter $2R = 3$ nm and the intertube distance $d = 0$–1 nm, at fixed pressure ($p = 0.4$, 1 bar and $p = 2.5$ bar, left to right). $T = 300$ K.
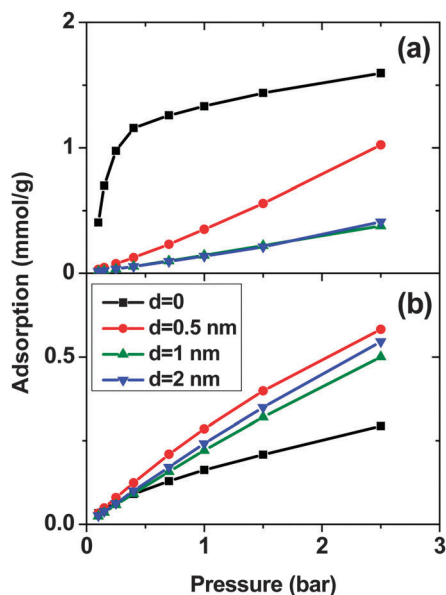
Fig. 5 Excess adsorption isotherms of (a) SO_2 and (b) N_2 in a binary mixture (1:99) on double-walled carbon nanotube arrays, with the inner tube diameter $2R = 3$ nm and the intertube distance $d = 0$–2 nm. $T = 303$ K.

Fig. 6 Selectivity of SO_2 over N_2, computed by the GCMC simulations, in a binary mixture (1:99) on double-walled carbon nanotube arrays, with the inner tube diameter $2R = 3$ nm and the intertube distance $d = 0$–2 nm. $T = 303$ K.

and CNT walls in the intertube space and also to the very low partial pressure of SO_2 ($p_{SO_2} < 0.025$ bar), which causes the limited intertube space to be large enough to accommodate the few SO_2 molecules. This result is in line with SO_2 adsorption isotherms in the SO_2–CO_2 system (Fig. 1), where $d = 0$ also has the maximum adsorption at low partial pressure ($p_{SO_2} < 0.025$ bar).

For N_2, $d = 0$ shows the lowest adsorption because most of the available volume, especially in the groove and interstitial regions, is occupied by SO_2 molecules which have stronger interactions with CNTs. However, N_2 adsorption increases uniformly with pressure, since N_2 molecules are smaller than SO_2 and they fit in the accessible space between SO_2 molecules. Increasing the intertube distance slightly to 0.5 nm has two important consequences. Firstly, the intertube volume increases and secondly, the density of SO_2 molecules decreases. As a result, there is more space accessible for N_2 molecules. Therefore, N_2 adsorption is notably higher at $d = 0.5$ nm than at $d = 0$. A further increase in the intertube distance reduces the interaction between N_2 molecules and DWCNT carbons which causes a decrease in the adsorption of N_2.

The adsorption of N_2 is generally less than SO_2 in all systems, although the bulk concentration of N_2 is much higher than SO_2. To investigate the reason we calculate the minimum energy of one single SO_2, CO_2 and N_2 molecule inside the CNT. For this purpose the probability of the Monte Carlo moves, displace, rotate, and insert/delete, is changed to 0.7, 0.3 and 0.0, respectively, and the simulation is carried out at low temperature (5 K). The minimum adsorption energies are -13 kJ mol^{-1}, -22.6 kJ mol^{-1} and -27.4 kJ mol^{-1} for one N_2, CO_2 and SO_2 molecule, respectively. Thus, the observed selectivity for SO_2 (Fig. 6) is mainly caused by the interaction of individual molecules with the CNT. The selectivity for the system with $d = 0$ increases initially with
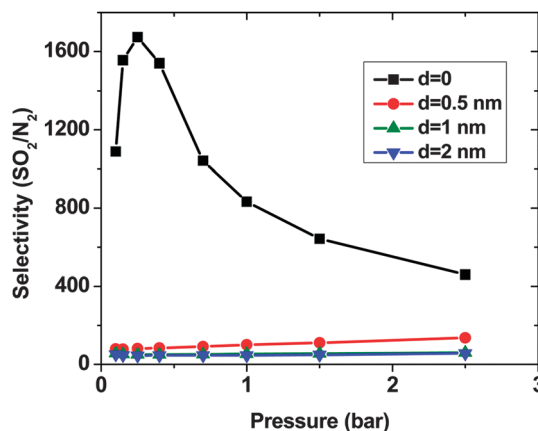
pressure, reaching a maximum of more than 1600 at $p = 0.25$ bar. Further increase of pressure leads to a decrease in selectivity, but at $p = 2.5$ bar it is still ~ 400. This is due to the fact that SO_2 is a large molecule with a strong interaction with CNT. Therefore, SO_2 molecules fill the intertube space soon at low pressure ($p < 0.4$ bar) and saturate the system. On the other hand, the small N_2 molecules can be accommodated between SO_2 molecules and thus, N_2 adsorption shows a monotonic increase as a function of pressure. The selectivity for the system with $d = 0.5$ nm increases smoothly from ~ 80 to ~ 140 with pressure. The selectivities of the other systems are almost constant ($S_{SO_2/N_2} \sim 55$ and ~ 45 for $d = 1$ nm and 2 nm, respectively) in the studied pressure region.

A comparison between GCMC simulations and IAST predictions in the SO_2–N_2 system is shown in Fig. 7. As for the SO_2–CO_2 system, IAST cannot predict the adsorption very well for $d = 0$. Because of the high density in the intertube space, the mixing behavior of the adsorbed gases is far from ideal. For larger d, the gas density decreases and as a consequence the IAST predictions become more similar to the adsorption calculated using simulations. Furthermore, the IAST predictions and GCMC results of the SO_2–N_2 mixture agree better than those of the SO_2–CO_2 mixture because of the weaker interaction of N_2 with either SO_2 or CNT carbons than that of CO_2.

3.3. CO_2–N_2 mixture

Fig. 8 shows the adsorption of CO_2–N_2 (15:85) mixtures calculated using the GCMC method and IAST predictions. When $d = 0$, there is an obvious deviation between IAST predictions and GCMC simulations but it is much less than what is observed in SO_2–CO_2 and SO_2–N_2 mixtures. Like the previous mixtures, in the systems with $d > 0$, the deviation between IAST and GCMC is less than that of $d = 0$. At $p = 2.5$ bar, the maximum deviation is less than 7% and 3% for CO_2 and N_2 respectively. In short, IAST can predict the CO_2–N_2 mixture better than SO_2–CO_2 and SO_2–N_2 mixtures. This result is in line with previous work.[19,21]

Similar to the SO_2–N_2 mixture, in all 4 CNT arrays, CO_2 shows higher adsorption than N_2 although in the bulk, there is

This journal is © the Owner Societies 2016

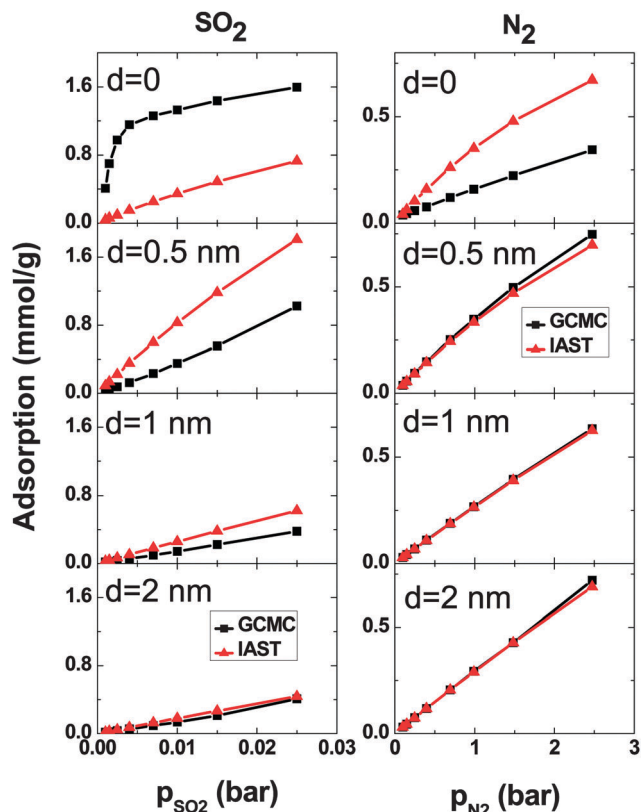*Phys. Chem. Chem. Phys.*, 2016, **18**, 4112–4120 | **4117**

Fig. 7 Comparison of excess adsorption data from IAST and GCMC simulations: SO_2 (left column) and N_2 (right column) in a binary mixture (1 : 99) on double-walled carbon nanotube arrays, with the inner tube diameter $2R = 3$ nm and the intertube distance $d = 0-2$ nm. $T = 303$ K.
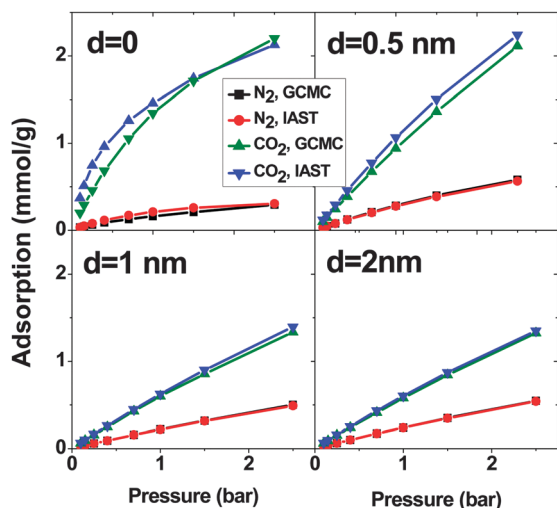

Fig. 8 Excess adsorption isotherms of CO_2 and N_2 in a binary mixture system on double-walled carbon nanotube arrays, with the inner tube diameter $2R = 3$ nm and the intertube distance $d = 0$, 0.5 nm, 1 nm and 2 nm. $T = 303$ K.

more N_2 than CO_2. This is due to the stronger interaction between CO_2 and CNTs (*cf.* Section 3.2). Moreover, $d = 0$ shows the highest difference between the N_2 and CO_2 adsorption. The selectivity highlights this difference (Fig. 9). The system with
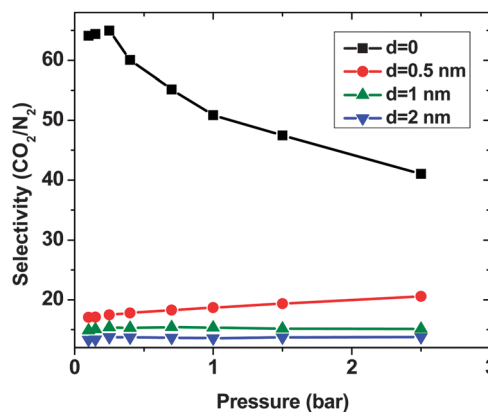

Fig. 9 Selectivity of CO_2 over N_2 (15 : 85), computed by the GCMC method, in a binary mixture system on double-walled carbon nanotube arrays, with the inner tube diameter $2R = 3$ nm and the intertube distance $d = 0-2$ nm. $T = 303$ K.

$d = 0$ has the highest selectivity. With increasing pressure, the limited adsorption space in this region causes the selectivity to decrease from around 70 to around 40 at $p = 2.5$ bar, which is still high. Unlike for $d = 0$, an increase in the pressure enhances the selectivity of CNTs with $d = 0.5$ nm. Nevertheless, the selectivity of this system is much lower (~ 20) than that with $d = 0$. For larger d, the system shows an almost constant selectivity (~ 15 and ~ 13 for $d = 1$ nm and 2 nm, respectively) in the studied pressure range and it is lower than for the two shorter intertube distances. Moreover, the observed selectivity of CO_2 over N_2 for optimized DWCNTs is higher than what has been reported for zeolites (between ~ 10 and ~ 30 depending on the type of zeolite and the pressure) and MOFs (between ~ 5 and ~ 40 depending on the type of MOFs and the pressure).[36,44]

3.4. Ternary mixture

To represent flue gas composition more realistically, we calculated the selectivity of a ternary mixture to CNT arrays with $d = 0.5$ nm (Fig. 10). The molar ratio of N_2–CO_2–SO_2 considered is 84.21 : 15 : 0.79, which is similar to ratios of studied binary mixtures in the present work. The selectivity of SO_2 over CO_2 increases with pressure from ~ 4.5 to ~ 7. This trend is very similar to what was observed for the SO_2–CO_2 binary mixture. This result was expected, since the interaction between N_2 and CNT is very weak in comparison with that between either SO_2 or CO_2 and the CNT. Thus, N_2 does not have an influence on the selectivity of SO_2 over CO_2. The selectivity of SO_2 over N_2 (and CO_2 over N_2) in a ternary mixture shows the same trend as in a binary mixture. The selectivities increase with pressure, however, in a ternary mixture, S_{SO_2/N_2} (S_{CO_2/N_2}), they are apparently higher than in a binary mixture. The presence of two species (CO_2 and SO_2), which are both more adsorptive than N_2, leads to an additional crowding-out of N_2 from adsorption sites and, as a result, higher selectivities.

4. Conclusion

In this work, we used grand-canonical Monte Carlo simulations to study the adsorption and separation properties of parallel-aligned
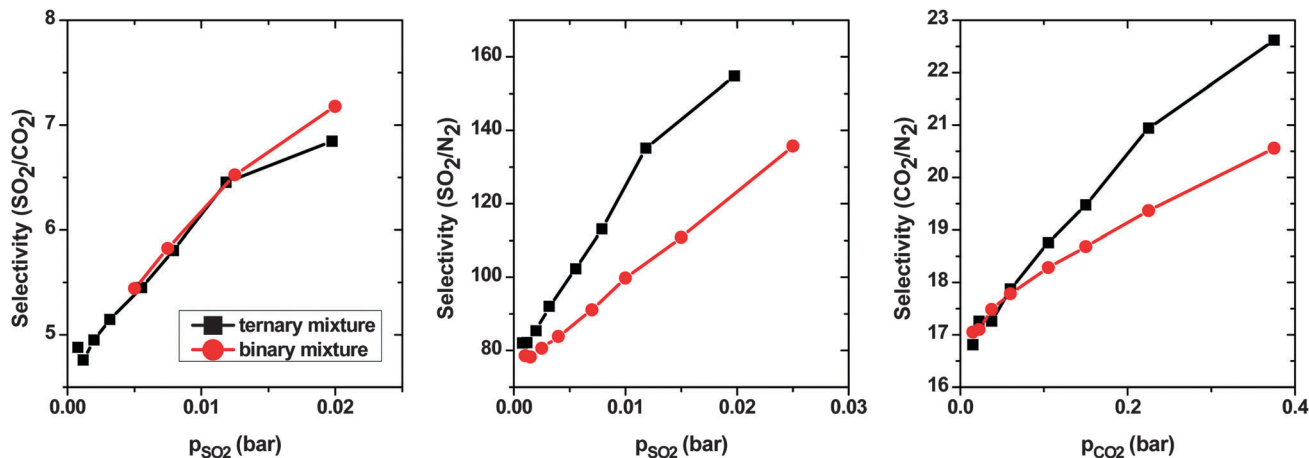
Fig. 10 Selectivity of SO_2 over CO_2 (right), SO_2 over N_2 (middle) and CO_2 over N_2 (left), computed by the GCMC method, in ternary and binary mixture systems on double-walled carbon nanotube arrays, with the inner tube diameter $2R = 3$ nm and the intertube distance $d = 0.5$ nm. $T = 303$ K.

DWCNTs for flue gas mixture components (SO_2, CO_2, and N_2) at 303 K. Bundles of DWCNTs with a constant inner diameter of $2R = 3$ nm but different intertube distances of $d = 0$–2 nm were studied.

The quantity and quality of the selectivity for each system depend on the type of adsorbate molecules and also on the adsorbent structure. For SO_2–CO_2 mixtures, the adsorption of CO_2 and SO_2 as a function of the intertube distance is non-linear. As a result, at low pressures $p < 0.8$ bar, bundles whose tubes touch each other ($d = 0$) show the highest selectivity towards SO_2. For higher pressures, bundles with a finite but short intertube distance ($d = 0.5$ nm) show the highest selectivity. For SO_2–N_2 and CO_2–N_2, on the other hand, no such pressure dependence is found and close-packed CNT bundles ($d = 0$) have the maximum selectivity towards SO_2 and CO_2, respectively, over the whole studied pressure range. The selectivity relates directly to the difference in the strength of interaction between each gas species and CNTs. The highest difference and consequently, the highest selectivity are observed between SO_2 and N_2, followed by CO_2 and N_2, and finally SO_2 and CO_2. The lowest and the highest observed selectivities are 4 and 16 for SO_2–CO_2, 50 and 1600 for SO_2–N_2, and 10 and 70 for CO_2–N_2, respectively. The overall picture does not change for a ternary mixture of all three gases, because the adsorption of N_2 is so much weaker than the other two gases that their adsorption equilibria are not influenced by the presence of N_2. The selectivity results indicate that firstly, DWCNTs are excellent materials for gas purification and secondly, optimizing the pore structure is very important to achieve the highest selectivity. Fortunately, close-packed bundles are easy to obtain[45] and show the highest selectivity in most cases.

The IAST predictions fail in predicting the adsorption for mixtures involving SO_2, in particular when $d = 0$. Increasing d reduces the deviation between IAST and GCMC in SO_2–CO_2 and SO_2–N_2 binary mixtures. Nevertheless, the results are still not in agreement, indicating that IAST is not suitable for the systems containing strongly interacting molecules like SO_2. In the case of CO_2–N_2, the IAST and GCMC are in good agreement and like the other two systems, as d increases, the deviation between GCMC and IAST reduces.

Acknowledgements

References

1 F. L. Darkrim, P. Malbrunot and G. P. Tartaglia, *Int. J. Hydrogen Energy*, 2002, **27**, 193–202.

2 J. Zhao, A. Buldum, J. Han and J. P. Lu, *Nanotechnology*, 2002, **13**, 195–200.

3 X. Ren, C. Chen, M. Nagatsu and X. Wang, *Chem. Eng. J.*, 2011, **170**, 395–410.

4 M. J. O'Connell, *Carbon Nanotubes: Properties and Applications*, CRC Taylor & Francis, Boca Raton, FL, 2006.

5 C. Lu, H. Bai, B. Wu, F. Su and J. F. Hwang, *Energy Fuels*, 2008, **22**, 3050–3056.

6 A. I. Skoulidas, D. M. Ackerman, J. K. Johnson and D. S. Sholl, *Phys. Rev. Lett.*, 2002, **89**, 185901.

7 L. Huang, L. Zhang, Q. Shao, L. Lu, X. Lu, S. Jiang and W. Shen, *J. Phys. Chem. C*, 2007, **111**, 11912–11920.

8 S. Furmaniak, A. P. Terzyk, P. A. Gauden, P. Kowalczyk and G. S. Szymański, *Chem. Phys. Lett.*, 2013, **578**, 85–91.

9 S. Jakobtorweihen and F. J. Keil, *Mol. Simul.*, 2009, **35**, 90–99.

10 P. Kowalczyk, S. Furmaniak, P. A. Gauden and A. P. Terzyk, *J. Phys. Chem. C*, 2010, **114**, 21465–21473.

11 Y. Yang, M. Rahimi, J. K. Singh, M. C. Böhm and F. Müller-Plathe, *J. Phys. Chem. C*, under review.

This journal is © the Owner Societies 2016

Phys. Chem. Chem. Phys., 2016, **18**, 4112–4120 | **4119**

12 Z. Nickmand, S. F. Aghamiri, M. R. Talaie Khozanie and H. Sabzyan, *Sep. Sci. Technol.*, 2014, **49**, 499–505.

13 D. N. Futaba, K. Hata, T. Yamada, T. Hiraoka, Y. Hayamizu, Y. Kakudate, O. Tanaike, H. Hatori, M. Yumura and S. Iijima, *Nat. Mater.*, 2006, **5**, 987–994.

14 M. Rahimi, J. K. Singh, D. J. Babu, J. J. Schneider and F. Müller-Plathe, *J. Phys. Chem. C*, 2013, **117**, 13492–13501.

15 M. Rahimi, J. K. Singh and F. Müller-Plathe, *J. Phys. Chem. C*, 2015, **119**, 15232–15239.

16 S. Agnihotri, J. P. B. Mota, M. Rostam-Abadi and M. J. Rood, *Carbon*, 2006, **44**, 2376–2383.

17 M. Bienfait, P. Zeppenfeld, N. Dupont-Pavlovsky, M. Muris, M. Johnson, T. Wilson, M. DePies and O. Vilches, *Phys. Rev. B: Condens. Matter Mater. Phys.*, 2004, **70**, 035410.

18 A. L. Myers and J. M. Prausnitz, *AIChE J.*, 1965, **11**, 121–127.

19 X. Peng, X. Cheng and D. Cao, *J. Mater. Chem.*, 2011, **21**, 11259–11270.

20 R. Babarao, Z. Hu, J. Jiang, S. Chempath and S. I. Sandler, *Langmuir*, 2007, **23**, 659–666.

21 P. Kowalczyk, *Phys. Chem. Chem. Phys.*, 2012, **14**, 2784–2790.

22 J. J. Cannon, T. J. H. Vlugt, D. Dubbeldam, S. Maruyama and J. Shiomi, *J. Phys. Chem. B*, 2012, **116**, 9812–9819.

23 X. Peng, D. Cao and W. Wang, *Chem. Eng. Sci.*, 2011, **66**, 2266–2276.

24 K. Vasanth Kumar and F. Rodríguez-Reinoso, *RSC Adv.*, 2012, **2**, 9671.

25 W. Wang, X. Peng and D. Cao, *Environ. Sci. Technol.*, 2011, **45**, 4832–4838.

26 M. Rahimi, D. J. Babu, J. K. Singh, Y.-B. Yang, J. J. Schneider and F. Müller-Plathe, *J. Chem. Phys.*, 2015, **143**, 124701.

27 W. D. Cornell, P. Cieplak, C. I. Bayly, I. R. Gould, K. M. Merz, D. M. Ferguson, D. C. Spellmeyer, T. Fox, J. W. Caldwell and P. A. Kollman, *J. Am. Chem. Soc.*, 1995, **117**, 5179–5197.

28 G. Hummer, J. C. Rasaiah and J. P. Noworyta, *Nature*, 2001, **414**, 188–190.

29 J. G. Harris and K. H. Yung, *J. Phys. Chem.*, 1995, 12021–12024.

30 M. H. Ketko, G. Kamath and J. J. Potoff, *J. Phys. Chem. B*, 2011, **115**, 4949–4954.

31 J.-C. Neyt, A. Wender, V. Lachet and P. Malfreyt, *J. Phys. Chem. B*, 2011, **115**, 9421–9430.

32 U. Essmann, L. Perera, M. L. Berkowitz, T. Darden, H. Lee and L. G. Pedersen, *J. Chem. Phys.*, 1995, **103**, 8577.

33 D.-Y. Peng and D. B. Robinson, *Ind. Eng. Chem. Fundam.*, 1976, **15**, 59–64.

34 P. Wattanaphan, T. Sema, R. Idem, Z. Liang and P. Tontiwachwuthikul, *Int. J. Greenhouse Gas Control*, 2013, **19**, 340–349.

35 A. Chakma, *Energy Convers. Manage.*, 1995, **36**, 427–430.

36 B. Liu and B. Smit, *J. Phys. Chem. C*, 2010, **114**, 8515–8522.

37 W. Sun, L.-C. Lin, X. Peng and B. Smit, *AIChE J.*, 2014, **60**, 2314–2323.

38 X. Xu, C. Song, R. Wincek, J. M. Andresen, B. G. Miller and A. W. Scaroni, *Fuel Chem. Div. Prepr.*, 2003, **48**, 162–163.

39 M. D. LeVan and T. Vermeulen, *J. Phys. Chem.*, 1981, **85**, 3247–3250.

40 A. Sharma, S. Namsani and J. K. Singh, *Mol. Simul.*, 2014, **41**, 414–422.

41 D. D. Do, H. D. Do, A. Wongkoblap and D. Nicholson, *Phys. Chem. Chem. Phys.*, 2008, **10**, 7293–7303.

42 A. Aqel, K. M. M. A. El-Nour, R. A. A. Ammar and A. Al-Warthan, *Arabian J. Chem.*, 2012, **5**, 1–23.

43 P. Kowalczyk, *Phys. Chem. Chem. Phys.*, 2012, **14**, 2784–2790.

44 B. Liu and B. Smit, *Langmuir*, 2009, **25**, 5918–5926.

45 D. J. Babu, M. Lange, G. Cherkashinin, A. Issanin, R. Staudt and J. J. Schneider, *Carbon*, 2013, **61**, 616–623.

4120 | *Phys. Chem. Chem. Phys.*, 2016, **18**, 4112–4120

This journal is © the Owner Societies 2016